Polym. Bull. (2015) 72:2241–2262
DOI 10.1007/s00289-015-1402-8

ORIGINAL PAPER

Synthesis of magnetic carboxymethyl chitosan-*g*-poly(acrylamide)/laponite RD nanocomposites with enhanced dye adsorption capacity

Gholam Reza Mahdavinia[1] · **Shiva Karami**[1]

Received: 17 February 2015 / Accepted: 18 May 2015 / Published online: 29 May 2015

Abstract This investigation reports the synthesis of magnetic nanocomposite hydrogels based on carboxymethyl chitosan-*g*-poly(acrylamide) (CMC-*g*-PAAm). The magnetic nanoparticles were prepared via in situ co-precipitation of iron salts in the presence of laponite RD nanoclay. Different contents of magnetic nanoclay were utilized to prepare magnetic CMC-*g*-PAAm nanocomposites. The structure of nanocomposite hydrogels was characterized by transmittance electron microscopy, scanning electron microscopy, X-ray diffraction, thermogravimetric analysis, and vibrating sample magnetometer techniques. The obtained magnetic nanocomposites were examined to remove crystal violet (CV) cationic dye from aqueous solutions. By introducing magnetic laponite RD, the nanocomposites showed an enhanced adsorption capacity for CV dye. Equilibrium adsorption data were modeled according to Langmuir and Freundlich isotherm models. The following experimental isotherm data from models was affected by the content of magnetic laponite RD. The maximum adsorption of crystal violet on magnetic nanocomposite hydrogels was 169 mg g^{-1}. In addition to high adsorption capacity of magnetic nanocomposites for CV, the regeneration of obtained adsorbents was effective and the corresponding nanocomposites may be considered as new candidate in the treatment of colored water.

Keywords Carboxymethyl chitosan · Magnetic · Laponite RD · Nanocomposite · Adsorption

✉ Gholam Reza Mahdavinia
gholamreza.mahdavinia@gmail.com; grmnia@maragheh.ac.ir

[1] Department of Chemistry, Faculty of Science, University of Maragheh, P.O. Box 55181-83111, Maragheh, Iran

Introduction

Synthetic dyes in large quantities are used by many industries such as textile, paper production, leather tanning, and food technology. Owing to the reactive functional groups on synthetic dyes (especially aromatic amines) not only enables them to be carcinogen, the toxicity of synthetic dye endangers the both human and aquatic life [1]. So, the dyes should be removed from the effluent of the mentioned technologies before discharging them into environment. Some current techniques used for removal of dyes from aqueous solutions include chemical precipitation, filtration, electrochemical treatment, reverse osmosis, and adsorption [2]. Because of ease of operation and good recycling susceptibility, the adsorption method is considered as an efficient and economic method to remove cationic and anionic dyes from aqueous solutions [3]. In this case, activated carbon [4], clay minerals [5], nanocomposites [6], and hydrogels [7] are often used. Hydrogels are three-dimensional crosslinked hydrophilic polymers that can absorb aqueous solutions without dissolving. Hydrogels can classify into non-ionic and ionic materials. The ionic types comprise anionic ($–CO_2^-$, $–SO_3^-$) or cationic ($–NR_3^+$) pendants [8]. The presence of these ionic groups in the hydrogels opens potential area of application particularly removal of pollutants from wastewater. The hydrogels composed of sodium alginate with carboxylate groups ($–CO_2^-$) [9], chitosan with amine pendants ($–NH_2$) [10], and kappa-carrageenan with anionic sulfate groups ($–OSO_3^-$) [7] have been synthesized and used as adsorbent to remove cationic dyes from aqueous solutions. Carboxymethyl chitosan, an important derivative of chitosan, is known as biopolymer which contains carboxylate ($–CO_2^-$) and amine ($–NH_2$) functional groups [11]. Owing to these functionalities, carboxymethyl chitosan is suggested as convenient functional matter, since this modified chitosan has good properties like biocompatibility, biodegradability, and adsorption properties [11]. It is also found to be valuable in some specialized applications, including adsorption of pollutants from aqueous solutions [12]. Carboxymethyl chitosan-based adsorbents such as neat carboxymethyl chitosan for adsorption of cationic dye [12, 13], entrapped carboxymethyl chitosan with silica for adsorption of neodymium ions [14], removal of congo red by carboxymethyl chitosan/montmorillonite nanocomposite [15], and adsorption of dyestuff on the carboxymethyl chitosan/polyvinyl alcohol [16] can be mentioned.

Recently, the use of magnetic adsorbents for removal of dyes from wastewaters is attractive due to the facile separation of adsorbents from solutions using a permanent magnet [17]. The common magnetic nanoparticles used for preparation of magnetic adsorbents are magnetite type of iron oxide (Fe_3O_4) which is synthesized from co-precipitation of Fe^{+2}/Fe^{+3} iron ions. The absence of reactive centers on magnetic particles restricts their application in wastewater treatments. Thus, magnetic nanoparticle-based-adsorbents are generally modified by polymers, organosilanes, and neat clays containing active anionic/cationic centers [14, 18–20]. These modifications improve the adsorption capacity of magnetic adsorbents because of introduced active centers. Laponite RD is a synthetic layered silicate

with anionic centers. The magnetic adsorbents based on laponite RD nanoclay have been synthesized and examined to remove cationic dye from aqueous solutions [20].

Nanocomposite adsorbents comprising only nanoclays [20] or magnetic Fe_3O_4 nanoparticles [18] have been applied to adsorb dye from wastes. There are just few reports in simultaneous incorporation of nanoclay and magnetite [21]. In this study, we attempt to synthesize the magnetic Fe_3O_4 nanoparticles through in situ co-precipitation of iron ions in the presence of laponite RD nanoclay. Then, the magnetic hydrogel nanocomposites of carboxymethyl chitosan-*g*-poly(acrylamide) were prepared by incorporation of magnetic laponite RD. The structure of magnetic nanocomposite hydrogels was characterized by scanning electron microscopy (SEM), transmittance electron microscopy (TEM), thermogravimetric analysis (TGA), X-ray diffraction (XRD), and vibrating sample magnetometer (VSM) techniques. The obtained magnetic nanocomposite hydrogels were examined for removal of crystal violet cationic dye from water. The isotherm and thermodynamic of adsorption process as well as the effects of salinity and pH on adsorption process were investigated.

Experimental

Materials

N,*O*-Carboxymethyl chitosan was obtained from Sigma-Aldrich Company (USA). The molecular weight and purity were 300,000 Da and 98 %, respectively. Laponite RD was provided by Rockwood Additive Limited (Surface area 370 m^2/g, bulk density 1000 kg/m^3, chemical composition: SiO_2 59.5 %, MgO 27.5 %, Li_2O 0.8 %, Na_2O 2.8 %, loss on ignition 8.2 %). Acrylamide (AAm) was purchased from Nalco Chemical Co. (Netherlands) and used after re-crystallization from acetone. *N*,*N*-Methylenebisacrylamide (MBA, Fluka) and ammonium persulfate (APS, Merck) were used as received. The other chemicals were analytical grades and used as received.

Synthesis of magnetic laponite RD

3 g of laponite RD was dispersed in 200 mL distilled water and stirred for overnight. The dispersed clay was sonicated for 10 min and the operating frequency used in sonication was 50 kHz. The iron salts (1.9 g $FeSO_4{\cdot}7H_2O$ and 3 g $FeCl_3{\cdot}6H_2O$; the Fe^{3+}:Fe^{2+} ratio was 1.5:1) were dissolved in 20 mL of distilled water. The solution of iron salts was added to the solution of laponite RD and was allowed to stir under N_2 gas for 1 h. Then, the ammonia solution (3 M) was slowly dropped into solution and allowed to reach the pH of solution to 11. The produced magnetic laponite RD was stirred at 70 °C for 2 h. The solution of magnetic laponite RD was cooled to ambient temperature. The produced magnetic laponite RD was separated by permanent magnet. The product was washed with distilled water for several times until neutralization.

Finally, the magnetic laponite RD was separated by magnet and the volume of solution was adjusted at 80 mL. The solution was sonicated for 10 min and a fluid solution was obtained. The magnetic fluid was used to synthesize magnetic nanocomposite hydrogels.

Synthesis of nanocomposite hydrogels

The magnetic carboxymethyl chitosan-*g*-poly(acrylamide)/laponite RD (mCMC-*g*-PAAmLap) was synthesized through grafting acrylamide monomer onto carboxymethyl chitosan in the presence of magnetic laponite RD and MBA crosslinker. The content of initial materials used to synthesize hydrogels is given in Table 1. In general, different volume of magnetic laponite RD fluid was poured in 40 mL of distilled water and allowed to stir for 24 h (speed of stirrer was 250 rpm). Then, the dispersed magnetic laponite solution was sonicated for 20 min. The operating frequency used in sonication was 75 kHz. Carboxymethyl chitosan (0.75 g) was poured in magnetic solution and stirred at ambient temperature until complete dissolving. 3 g of AAm monomer and 0.03 g of MBA (dissolved in 2 mL of distilled water) were poured in magnetic carboxymethyl chitosan solution. The obtained solution was sonicated for 5 min with the operating frequency of 25 kHz. Finally, APS initiator (0.1 g in 2 mL water) was added to the solution. After 2 h, the synthesized nanocomposite hydrogels were cut into small pieces and immersed in excess distilled water for purification. The purified nanocomposites were dried at 40 °C in an oven for constant weight. The dried samples were milled and sieved to 40–60 mesh sizes and kept away from light and moisture. The non-magnetic hydrogel (CMC-*g*-PAAm) was synthesized as above without using magnetic laponite RD fluid.

Swelling measurements

The degree of swelling (DS) was determined by immersing dried nanocomposite hydrogels (0.1 g) in distillated water (100 mL) or 0.15 M of salt solutions (50 mL) and was allowed to soak at room temperature for 24 h. After this time, they were removed from water, blotted with filter paper to remove surface water, weighed and the DS (g water/g dried nanocomposite) was calculated using Eq. 1:

Table 1 Required contents of initial materials used to synthesize magnetic nanocomposite hydrogels

	Magnetic laponite RD (mL)	Carboxymethyl chitosan (g)	AAm (g)	MBA (g)	APS (g)
CMC-*g*-PAAm	0	0.75	3	0.03	0.1
mCMC-*g*-PAAmLap1	5	0.75	3	0.03	0.1
mCMC-*g*-PAAmLap2	10	0.75	3	0.03	0.1
mCMC-*g*-PAAmLap3	20	0.75	3	0.03	0.1
mCMC-*g*-PAAmLap4	30	0.75	3	0.03	0.1

$$\mathrm{DS} = \frac{W_\mathrm{s} - W_\mathrm{d}}{W_\mathrm{d}}, \quad (1)$$

where W_s and W_d are the weights of the samples swollen in aqueous solutions and in dry state, respectively.

Dye adsorption measurements

Adsorption of CV on nanocomposites was carried out by immersing 0.05 g of nanocomposites into 50 mL of dye solution with 60 mg L^{-1} of CV. All adsorption experiments were carried out through a batch method on a shaker with a constant speed at 120 rpm. All adsorption experiments were done at ambient temperature (24 °C). To study the effect of time on adsorption, at specified time intervals, the amount of adsorbed CV was evaluated using a UV spectrometer at $\lambda_{\max} = 595$ nm. The removed solutions were centrifuged (at 3000 rpm for 10 min) before measurements. The content of adsorbed dye was calculated using Eq. 2:

$$q_t = \frac{(C_0 - C_t)}{m} \times V, \quad (2)$$

where C_0 is the initial CV concentration (mg L^{-1}), C_t is the remaining dye concentration in the solution at time t, V is the volume of dye solution used (L), and m is the weight of nanocomposite (g). Adsorption isotherm was carried out by immersing 0.05 g of nanocomposites into 50 mL of dye solutions with 10, 30, 60, 90, 140, and 200 mg L^{-1} of CV at ambient temperature (24 °C) for 24 h. The equilibrium adsorption capacity of nanocomposites, q_e (mg g^{-1}), was determined using Eq. 2. At this equation, the C_t and the q_t will be replaced with equilibrium concentration of dye in the solution (C_e) and equilibrium adsorption capacity (q_e), respectively.

The removal efficiency (RE %) of CV by nanocomposites was calculated as below:

$$\mathrm{RE}\ \% = \frac{C_0 - C_\mathrm{e}}{C_0} \times 100, \quad (3)$$

where C_e is the remaining CV concentration in the solution at equilibrium time.

Desorption studies

Desorption study was carried out via bath method. The desorption solutions in this study were ethanol (96 % v/v), water/ethanol (50/50 v/v), 0.5 M KCl in water, 0.5 M KCl in water/ethanol (50/50 v/v), and 0.2 M acetic acid solutions. The dye-loaded mCMC-*g*-PAAmLap4 nanocomposite was transferred into distilled water for 1 h to remove undesorbed dye. Then, the sample was immersed into desorption solution and stirred on a shaker (120 rpm) for 24 h. Desorption content was calculated according to the calibration curve for each solution.

Point of zero charge

The points of zero charge (pH_{pzc}) of hydrogels were determined according to our previous work [22]. In this series of experiments, 20 mL of 0.05 M of NaCl solution was poured into several beakers and the pH of NaCl solutions was adjusted from 1 to 11 by adding either 0.1 M of HCl or 0.1 M of NaOH solutions. After setting the pH, the volume of the solutions was adjusted to 30 mL by adding 0.05 M of NaCl solution. The initial pH (pHi) of the solutions was exactly recorded and the solutions were transferred in Erlenmeyer flasks. Then, 50 mg of hydrogels was immersed into solutions and was shaken on a shaker (90 rpm, ambient temperature) for 48 h. The solutions containing hydrogels were centrifuged (4500 rpm) for 15 min and the pH of supernatant solution was recorded (pH_f). The points of zero charge were found from plot of ΔpH ($pH_i - pH_f$) versus pH_i.

Structural analysis

Dried nanocomposites were coated with a thin layer of gold and imaged in a SEM instrument (Vega, Tescan). One-dimensional, wide angle XRD patterns were obtained using a Siemens D-500 X-ray diffractometer with wavelength, $\lambda = 1.54$ Å (Cu-κα), at a tube voltage of 35 kV, and tube current of 30 mA. Transmission electron microscopy (TEM) micrographs were recorded with a Philips CM10 operating at 60 kV tension. The magnetic properties of the beads were studied with a VSM (model 7400, Lake Shore Company, USA). Thermal gravimetry analysis (Mettler Toledo, USA) was performed under N_2 atmosphere with the heating rate of 5 °C/min.

Results and discussion

Synthesis and characterization

Magnetic nanocomposite hydrogels were synthesized through grafting acrylamide onto carboxymethyl chitosan by incorporation of magnetic laponite RD. The Fe_3O_4 magnetic nanoparticles were synthesized via in situ co-precipitation of iron ions in the presence of laponite RD nanoclay. Then, the magnetic laponite RD fluid was added to the carboxymethyl chitosan solution, and magnetic nanocomposites were obtained after adding acrylamide, methylenebisacrylamide, and initiator. In our previous work, we reported the synthesis of hydrogel nanocomposites, where neat laponite RD was used as a crosslinker instead of MBA crosslinker [23]. After magnetizing of the laponite RD, it was examined as crosslinker. But the apparent strength of the nanocomposite hydrogels was not enough and thus we tried to utilize MBA crosslinker. The magnetic nanocomposite hydrogels were characterized by VSM, XRD, TEM, TGA, and SEM/EDS techniques.

VSM, SEM/EDS studies

The hysteresis loops of dried magnetic laponite RD and magnetic nanocomposite hydrogel (mCMC-*g*-PAAmLap4) were investigated between ±9 kOe at 298 K. The results are shown in Fig. 1a. According to data, the saturation magnetizations of magnetic laponite RD and mCMC-*g*-PAAmLap4 hydrogel were obtained 5.2 and 1.4 emu g^{-1}, respectively. The decrease in saturation magnetization of magnetic nanocomposite can be related to the coating effect of crosslinked hydrogel on magnetic nanoparticles. After adsorption process, the obtained saturation magnetization of the nanocomposite hydrogels was sufficient to separate them from aqueous solution by a permanent magnet (insert in Fig. 1a).

The surface microstructure of the magnetic-free hydrogel (CMC-*g*-PAAm, Fig. 1b) and magnetic hydrogel nanocomposite (mCMC-*g*-PAAmLap4, Fig. 1c) was studied by SEM technique. The introducing magnetic laponite RD did not affect significantly the morphology of magnetic hydrogel. For both hydrogels, a dense and relatively smooth surface was observed. Besides, the energy-dispersive X-ray spectroscopy (EDS) of the mCMC-*g*-PAAmLap4 was studied and the spectrum is shown in Fig. 1d. The characteristic peak of Fe is assigned to the magnetite nanoparticles. Also, distinctive peaks of magnesium, aluminum, and silicon were appeared in EDS spectrum of mCMC-*g*-PAAmLap4 that are assigned to the laponite RD. These results confirmed the presence of magnetic laponite RD in the hydrogel nanocomposite.

XRD, TEM, and TGA studies

The XRD patterns of neat laponite RD, magnetic laponite RD, and mCMC-*g*-PAAmLap4 hydrogel nanocomposite were studied and the results are shown in Fig. 2a. The XRD profile of pristine laponite RD showed a broad peak from $2\theta = 2.5°$ to $2\theta = 8°$ with a diffraction peak at about $2\theta = 6.1°$ which is assigned to the clay plates with d-spacing 14.2 Å. When the Fe_3O_4 nanoparticles were formed, the characteristic peak of laponite RD at $2\theta = 6.1°$ was disappeared. In the synthesis of magnetic laponite RD, the cation exchange can be occurred between Na^+ in clay and Fe^{3+} (or Fe^{2+}), and the synthesized Fe_3O_4 nanoparticles can be located between clay plates as well as on the surface of clay [20]. The existence of magnetic Fe_3O_4 in the magnetic laponite RD clay was confirmed by the characteristic peaks at about $2\theta = 30.5$, 35.5, 57.5 and 62.5 [24]. The interplanar distances were calculated according to Bragg's equation and found to be 2.91 Å ($2\theta = 30.5°$), 2.523 Å ($2\theta = 35.5°$), 1.606 Å ($2\theta = 57.5°$), and 1.48 Å ($2\theta = 62.5°$). The obtained results were in agreement with the database in JCPDS file (PDF No. 65-3107 [24]) and indicated the formation of highly crystalline and pure magnetite nanoparticles with spinel structure. Similar to magnetic laponite RD, the XRD pattern of magnetic nanocomposite hydrogel showed characteristic peaks at $2\theta = 30.5$, 35.5, 57.5 and 62.5 related to the Fe_3O_4 nanoparticles.

The TEM image of mCMC-*g*-PAAmLap4 nanocomposite hydrogel was studied and the result is shown in Fig. 2b. The laponite RD showed the platelets with a lateral size of 30–70 nm with thickness about 3 nm (according to XRD results). The

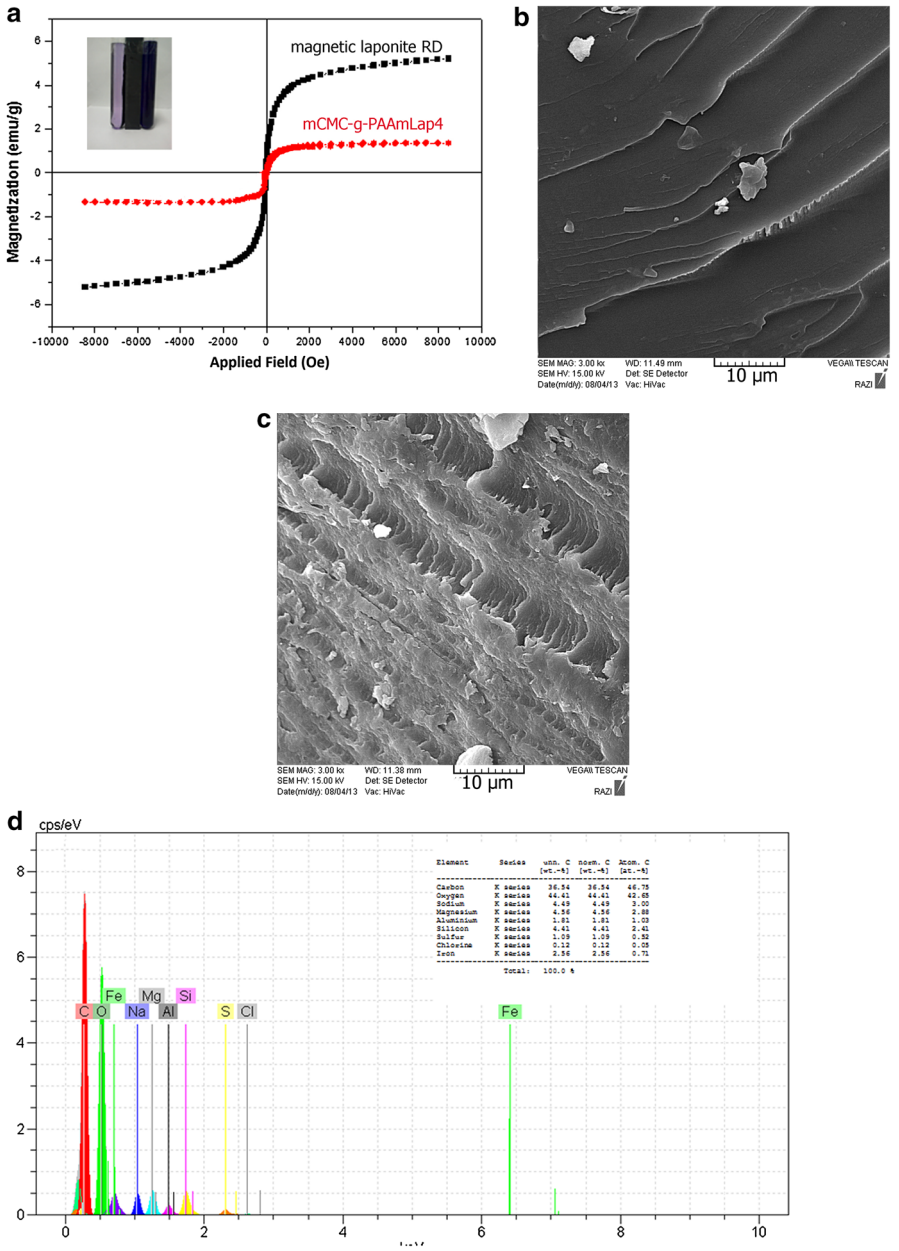

Fig. 1 **a** Hysteresis loops of magnetic laponite RD (mLap) and mCMC-*g*-PAAmLap4 (mCMCLap4) samples according to applied field at 298 K, **b** SEM micrograph of CMC-*g*-PAAM, **c** SEM micrograph of mCMC-*g*-PAAmLap4, **d** EDS graph of mCMC-*g*-PAAmLap4

magnetite nanoparticles (with the size of lower than 3 nm) were found to be embedded with clay plates. The absence of free magnetic nanoparticles can be arisen from the cation exchangeability of laponite RD that helps the nanoparticles to form on the surface and between plates of laponite RD. A similar observation has been reported by Tzitzios et al., where magnetic nanoparticles have been immobilized on laponite RD discs [25].

Thermal behaviors of CMC-*g*-PAAm and mCMC-*g*-PAAmLap3 hydrogels were studied and their TGA thermograms are shown in Fig. 2c. The first weight loss (~1.5 % for CMC-*g*-PAAm and ~2 % for CMC-*g*-PAAmLap3) occurred up to 200 °C due to the adsorbed water. The weight loss behavior of CMC-*g*-PAAm sample at second stage was obtained different from mCMC-*g*-PAAmLap3 nanocomposite hydrogel. At this stage, ~22 % of weight loss for CMC-*g*-PAAm occurred at 200–248 °C with a maximum decomposition rate at 237 °C. By introducing magnetic clay, the range of weight loss was shifted to 245–312 °C with a maximum decomposition rate at 270 °C. This observation indicated the improved thermal stability of magnetic hydrogel nanocomposite due to Fe_3O_4/laponite RD [26, 27]. Compared with CMC-*g*-PAAm, in the third stage, the weight loss of mCMC-*g*-PAAmLap3 was occurred with slower slope showing high thermal stability of magnetic hydrogel nanocomposite. The difference in the percent weight loss of non-magnetic and magnetic hydrogels up to 600 °C was approximately 7.8 %. This value could be attributed to the percent of Fe_3O_4/laponite RD in hydrogel matrix.

Swelling study

The degree of swelling of the hydrogel nanocomposites in distilled water as well as in salt solutions was investigated and the results are tabulated in Table 2. The water-absorbing capacity of hydrogel nanocomposites was affected by the content of magnetic laponite RD. In distilled water, swelling capacity of hydrogels was decreased as the amount of magnetic laponite RD increased. The maximum and minimum water-absorbing capacity was found to be 32.6 and 2.4 g g^{-1} for CMC-*g*-PAAm and mCMC-*g*-PAAmLap4, respectively. This decrement in water absorbency can be attributed to the interactions between polymer chains and laponite RD (or magnetite nanoparticles) that causing more physical crosslinking points, and thereby the water absorbency is decreased [23, 28].

The swelling ratio of anionic hydrogels is remarkably affected by the electrolytes. So, we attempt to study the swelling behavior of hydrogels in 0.15 M of different salt solutions (Na^+, Ca^{2+}, and Al^{3+}) with the same Cl^- counter ions (Table 2). The Ca^{2+} and Al^{3+} solutions had significant effect on the degree of swelling of hydrogels. This behavior is originated from the coordination of the Ca^{2+} and Al^{3+} cations with anionic centers of hydrogels [29]. Unlike aqueous solutions contained Ca^{2+} and Al^{3+} ions, the nanocomposites showed less decrease in swelling capacity in NaCl solution especially when the magnetic laponite RD was high. This behavior may be originated from nano-sized laponite RD plates, which lead to an enhancement in osmotic pressure inside the nanocomposites [30].

To have a comparative data, a dimensionless salt sensitivity factor, *f*, was determined using Eq. 4 [31]:

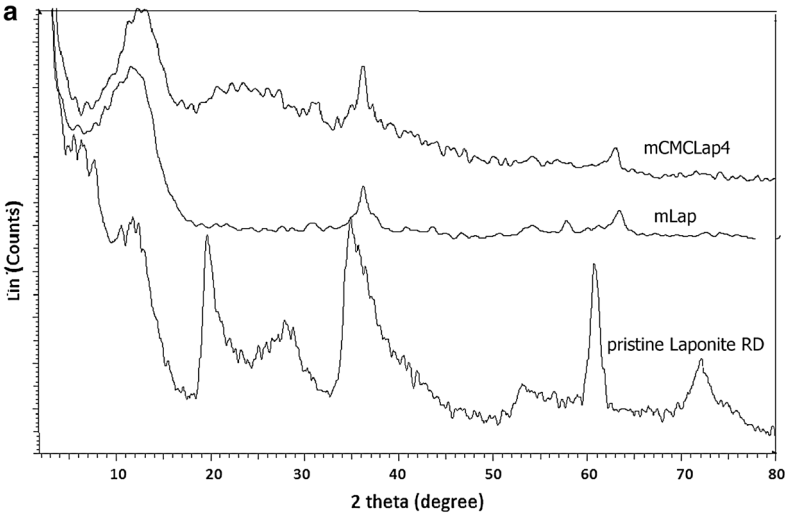
a
mCMCLap4
mLap
pristine Laponite RD
Lin (Counts)
10
20
30
40
50
60
70
80
2 theta (degree)

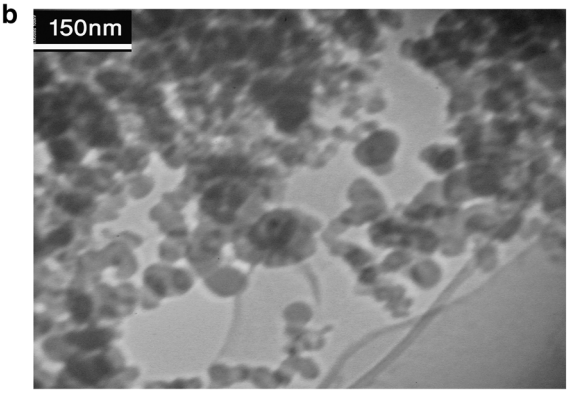
b
150nm

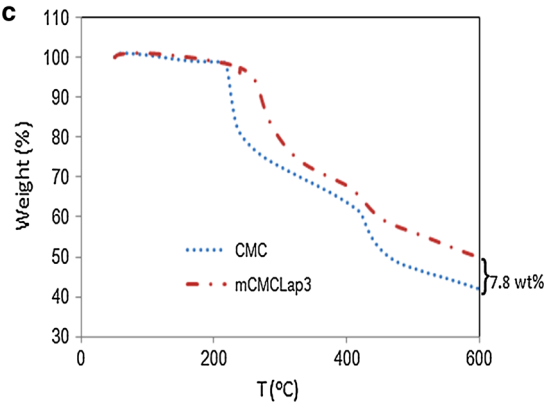
c
110
100
90
80
70
60
50
40
30
Weight (%)
CMC
mCMCLap3
7.8 wt%
0
200
400
600
T (°C)

◀**Fig. 2** **a** XRD patterns of pristine laponite RD, magnetic laponite RD (mLap), and mCMC-*g*-PAAmLap4 (mCMCLap4), **b** TEM images of mCMC-*g*-PAAmLap4 nanocomposite hydrogel, **c** TGA thermograms of CMC-*g*-PAAm (CMC) and mCMC-*g*-PAAmLap3 (mCMCLap3) hydrogels

Table 2 Degree of swelling and salt sensitivity (*f* values) of nanocomposite hydrogels in distilled water and 0.15 M of salt solutions

	DS_{H2O}	DS_{NaCl}	DS_{CaCl2}	DS_{AlCl3}	f_{NaCl}	f_{CaCl2}	f_{AlCl3}
CMC-*g*-PAAm	32.6	13	4.2	2.4	0.6	0.87	0.92
mCMC-*g*-PAAmLap1	14.2	11.5	10.4	2.4	0.19	0.26	0.83
mCMC-*g*-PAAmLap2	9.8	9.2	8.2	2.8	0.06	0.16	0.71
mCMC-*g*-PAAmLap3	4.6	4.2	4	1.6	0.08	0.13	0.65
mCMC-*g*-PAAmLap4	2.4	2.8	1.6	2.2	0.17	0.33	0.08

$$f = 1 - \frac{S_s}{S_w}, \tag{4}$$

where S_s and S_w are swelling in desired salt solution and in distilled water, respectively. The *f* values are also given in Table 2. Generally, in ionic nanocomposite hydrogels, the swelling capacity is decreased in saline media. Water uptake of carboxymethyl chitosan-based nanocomposites in saline was high and the *f* values were obtained lower than 0.1 and 0.35 in NaCl and $CaCl_2$ solutions, respectively. The low *f* values indicated the lowest salt sensitivity of related nanocomposites and can be considered as anti-salt nanocomposite hydrogels. This behavior was similar to our previous work that reported the swelling behavior of HPMC/laponite RD nanocomposites [32].

Dye adsorption studies

Effect of contact time

The removal rates of pollutants by adsorbents are useful data to predict the required time of removal, which present the information about the efficiency of adsorption process. Hence, the influence of contact time on the removal efficiency of CV by nanocomposites was investigated by immersing 0.05 g of adsorbents in 50 mL of CV solution (60 mg L^{-1}). The rates of adsorption of CV on hydrogels are shown in Fig. 3. Contact time plots indicated a relatively rapid removal rate. During the first 15 min, the removal efficiencies of dye by samples were obtained 65 (CMC-*g*-PAAm), 80.7 (mCMC-*g*–*g*-PAAmLap1), 82 (mCMC-*g*-PAAmLap2), 85 (mCMC-*g*-PAAmLap3), 86.7 % (mCMC-*g*-PAAmLap4). The adsorption equilibration was obtained by 60 min and the removal efficiencies were obtained 74 (CMC-*g*-PAAm), 87.6 (mCMC-*g*-PAAmLap1), 93.1 (mCMC-*g*-PAAmLap2), 99.1 (mCMC-*g*-PAAmLap3), 99.3 % (mCMC-*g*-PAAmLap4). The results showed that introducing magnetic laponite RD not only caused an improvement in rate of dye adsorption, but also the content of adsorbed CV on nanocomposites increased.

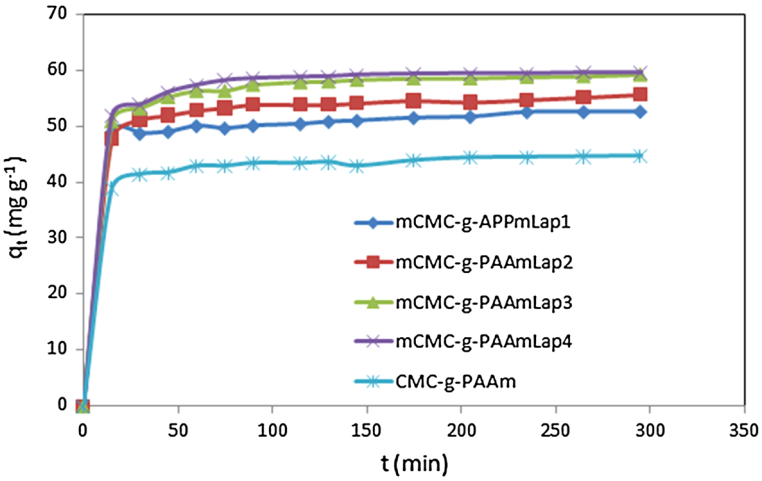

Fig. 3 Effect of contact time on the adsorption of CV onto nanocomposites (initial dye concentration 60 mg L^{-1}, dosage 50 mg, volume of dye solution 50 mL)

Effect of salinity and pH on adsorption

The adsorption capacities of adsorbents can be affected by the ion strength of dye solutions [33]. To investigate the effect of salinity on the adsorption capacities of hydrogels, the salinity of dye solution (60 mg L^{-1}) was adjusted by NaCl. The concentration of NaCl was changed from 0.01 to 0.5 M. Depending on the content of magnetic laponite RD, the adsorption of CV on corresponding samples showed different trends as indicated in Fig. 4a. It is clear from figure that the CV adsorption on mCMC-*g*-PAAmLap4 remained invariant with an increase in the NaCl concentration. In contrast, a decrement was found for the CV adsorption on the CMC-*g*-PAAm and mCMC-*g*-PAAmLap1. This difference may be explained by the swelling behavior of adsorbents in NaCl solution. The corresponding reduction of CV adsorption on the CMC-*g*-PAAm and mCMC-*g*-PAAmLap1 can be attributed to the low swelling of adsorbents in NaCl solutions (Table 2). The low swelling of CMC-*g*-PAAm and mCMC-*g*-PAAmLap1 leads to a decreased surface area and so a reduction in adsorption of dye on hydrogels is observed. According to Table 2, contrary to the CMC-*g*-PAAm and mCMC-*g*-PAAmLap1 hydrogels, the degree of swelling of mCMC-*g*-PAAmLap4 in NaCl solution was higher than that of distilled water, and results an increased surface area.

In addition to ion strength of dye solution, the effect of the pH of initial dye solution on the adsorption capacity of adsorbents was studied. The pH of initial dye solution is an important parameter influencing the adsorption of dyes onto adsorbents. To investigate the influence of pH, the pH of dye solutions changed from 2 to 10 and the results are indicated in Fig. 4b. By varying the pH, the results revealed that the presence of magnetic laponite RD affected significantly the adsorption of CV on adsorbents. The variation in dye adsorption capacity of magnetic-free hydrogel CMC-*g*-PAAm was remarkable. The dye adsorption

capacity of CMC-*g*-PAAm enhanced from 7 to 41 mg g^{-1} when the pH of solution was increased from 2 to 4. Then, the removal efficiency was remained relatively constant by increasing the pH of initial dye solution from 4 to 7. The low adsorption of CV dye on CMC-*g*-PAAm hydrogel in the pH ranged 2–4 can be attributed to the conversion of $–COO^-$ and $–NH_2$ to –COOH and $–NH_3^+$ groups and subsequent decrease in swelling of hydrogel. Besides, the cationic character of hydrogels due to the $–NH_3^+$ restricts the closing of cationic CV on adsorbents, and this results in a decrement in dye adsorption capacity of hydrogels. As the magnetic laponite RD introduced into hydrogels, the adsorption capacity of nanocomposites was improved under acidic media. For obtaining the reliability of this behavior of hydrogels, the pH_{pzc} of CMC-*g*-PAAm, mCMC-*g*-PAAmLap2, and mCMC-*g*-PAAmLap4 was determined and found about 6.3, 5.05, and 4.12, respectively (Fig. 4c). When the pH of dye solutions is higher than that of pH_{pzc}, the hydrogels comprise a negative surface charge in aqueous solutions and electrostatic interactions between cationic dye and negative center on the surface of adsorbents occur [34]. But at lower pH value than pH_{pzc}, the positive surface charge on adsorbents restricts the adsorption of cationic dye and thereby decreases adsorption capacity of samples. The improvement of dye adsorption in acidic media by nanocomposites can be attributed to the decrease in pH_{pzc} of nanocomposites.

Adsorption isotherms

The influence of initial CV concentration on the adsorption capacity of nanocomposites was investigated. The results can be used to study the adsorption isotherm that explains the correlation between the content of adsorbed dye on nanocomposites and the remained dye in solution at equilibrium time. Figure 5 indicates the relationship between equilibrium adsorption capacity of CMC-*g*-PAAm and mCMC-*g*-PAAmLap4 and the remaining dye in solution. At lower initial CV concentration, the main fraction of dye is adsorbed on the adsorbents; whereas at higher dye concentration, the adsorption capacity of hydrogels remains constant that can be attributed to the saturation of active centers on adsorbents. The types of interactions between adsorbate molecules and adsorbent surface can be studied by adsorption isotherms [35]. The experimental data were discussed according to non-linear Langmuir and Freundlich isotherm models. In the Langmuir adsorption model, adsorption of adsorbate takes place at specific homogeneous sites within the adsorbent and is valid for monolayer adsorption on adsorbents. The expression of the applied non-linear Langmuir model is given by the Eq. 5 [36, 37]:

$$q_e = \frac{q_m K_L C_e}{1 + K_L C_e}, \tag{5}$$

where C_e is the equilibrium dye concentration in the solution (mg L^{-1}) at equilibrium, K_L is the Langmuir adsorption constant related to the energy of adsorption (L mg^{-1}), and q_m is the maximum adsorption capacity (mg g^{-1}).

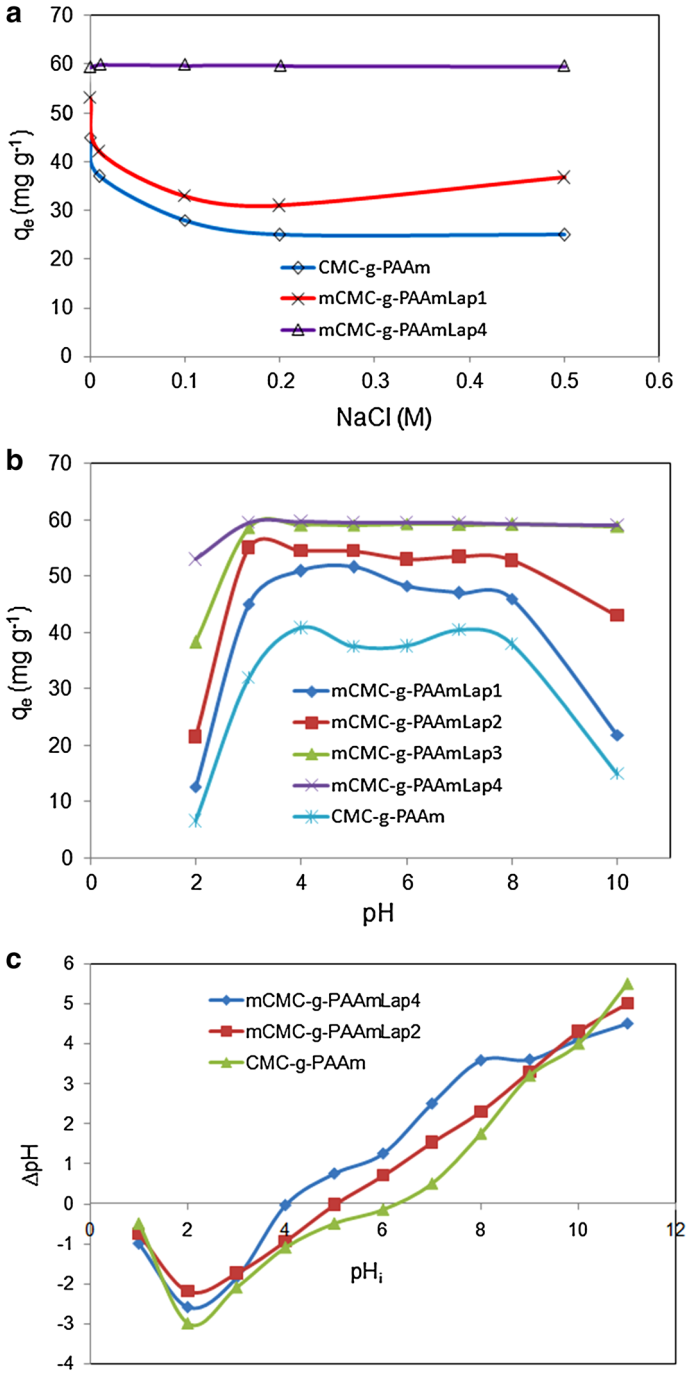
a
q_e (mg g^{-1})
NaCl (M)
CMC-g-PAAm
mCMC-g-PAAmLap1
mCMC-g-PAAmLap4
b
q_e (mg g^{-1})
pH
mCMC-g-PAAmLap1
mCMC-g-PAAmLap2
mCMC-g-PAAmLap3
mCMC-g-PAAmLap4
CMC-g-PAAm
c
ΔpH
pH_i
mCMC-g-PAAmLap4
mCMC-g-PAAmLap2
CMC-g-PAAm

◀**Fig. 4** **a** Effect of NaCl concentration on the adsorption of dye on nanocomposite hydrogels, **b** Effect of pH of initial dye solution on the adsorption of dye on nanocomposite hydrogels, **c** points zero charge of CMC-*g*-PAAm, mCMC-*g*-PAAmLap2 and mCMC-*g*-PAAmLap4 hydrogels

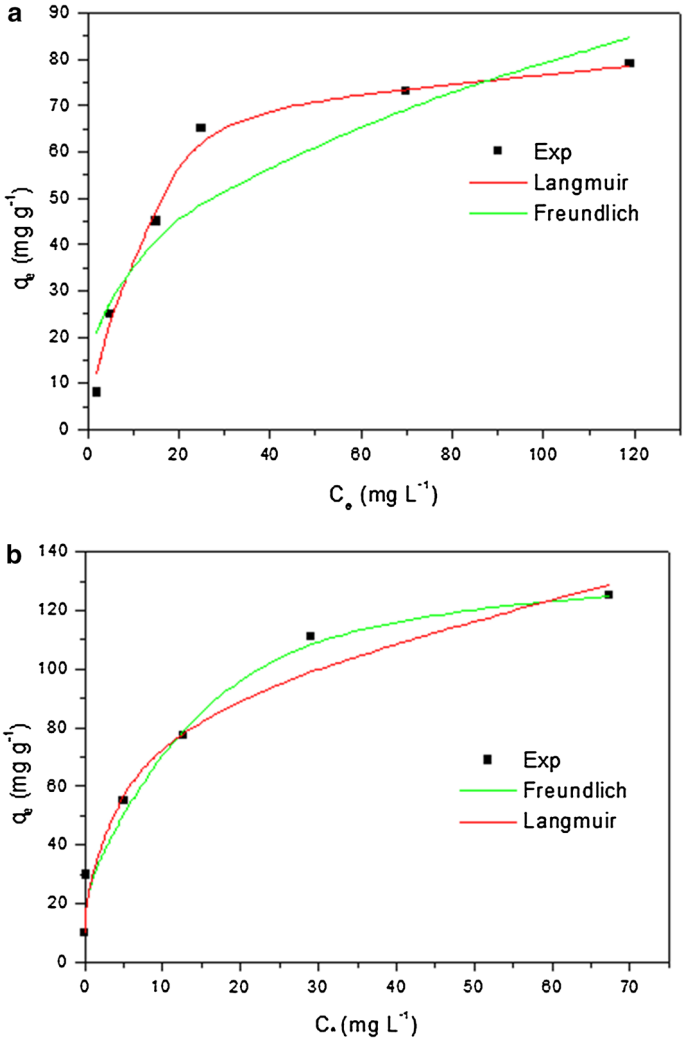

Fig. 5 Langmuir and Freundlich isotherm models according to non-linear method for adsorption of CV onto **a** CMC-*g*-PAAm and **b** mCMC-*g*-PAAmLap4

In the Freundlich model, the adsorption of adsorbate occurs on a heterogeneous surface by multilayer sorption and the adsorption capacity can increase with an increase in adsorbate concentration. Non-linear Freundlich isotherm is represented by the following equation [36]:

$$q_e = k_F C_e^{1/n}, \quad (6)$$

where k_F is the equilibrium adsorption coefficient (mg g^{-1}) (L mg^{-1})$^{1/n}$, and *1/n* is the empirical constant. In fact, the *n* value depicts the favorability of adsorption process and k_F is the adsorption capacity and intensity of the adsorbate.

The non-linear fitting of data was performed using Origin 8 software. The validity of models was estimated by regression coefficient (r^2) and Chi-square test (χ^2) that obtained from the analysis of variance (ANOVA) in Origin. A well fitting occurs when the r^2 is close to unity and χ^2 be the lowest [36].

The adsorption of CV onto CMC-*g*-PAAm and mCMC-*g*-PAAmLap4 fitted to the Langmuir and Freundlich isotherm models is shown in Fig. 5. While the experimental data of CMC-*g*-PAAm fitted well the Langmuir model, a contrary trend was observed for mCMC-*g*-PAAmLap4 with well fitting to the Freundlich model. The adsorption constant parameters as well as the r^2 and χ^2 obtained after fitting are summarized in Table 3. The r^2 and χ^2 values demonstrated that the agreement of isotherm models with experimental data was affected by the content of introduced magnetic laponite RD. According to the r^2 and χ^2 values, while the adsorption of CV on CMC-*g*-PAAm and mCMC-*g*-PAAmLap1 followed well the Langmuir model, by increasing the magnetic laponite RD, the fitting of practical data deviated from Langmuir and the data correlated well with Freundlich isotherm model. The experimental maximum ($q_{m,exp}$) adsorption capacities of CMC-*g*-PAAm and mCMC-*g*-PAAmLap1 hydrogels were relatively in agreement with the theoretical adsorption capacity from Langmuir model (q_m), which confirmed the best fit of Langmuir model with practical data.

In the hydrogels with the high content of magnetic laponite RD (mCMC-*g*-PAAmLap2, mCMC-*g*-PAAmLap3 and mCMC-*g*-PAAmLap4), the chi-square χ^2 and r^2 values were consistent with Freundlich model. In Freundlich model, when the *n* values being between 1 and 10, the removing process will be beneficial adsorption. The *n* values for samples were greater than 1 and

Table 3 Constants of isotherm models for adsorption of CV on nanocomposite hydrogels

Isotherm	CMC-*g*-PAAm	MCMC-*g*-PAAmLap1	MCMC-*g*-PAAmLap2	MCMC-*g*-PAAmLap3	MCMC-*g*-PAAmLap4
Freundlich					
n	2.93	2.75	3.5	4.08	5.02
k_F	16.5	24.65	38.6	59.23	86.7
r^2	0.88	0.94	0.97	0.92	0.94
χ^2	0.25	0.4	0.02	0.31	0.05
Langmuir					
q_m	80.6	122.2	138.8	137	156.4
K_L	0.08	0.069	0.123	0.69	1.74
r^2	0.98	0.97	0.92	0.83	0.89
χ^2	~0	0.078	0.54	3.49	1.9
$q_{m,exp}$	79	120	132	153	169

indicated the favorability of the adsorption process. The enhanced adsorption capacity of nanocomposite hydrogels due to the introduced high content of magnetic laponite RD may be attributed to the well correlation of experimental data with Freundlich model. In our previous works, we reported nanocomposite hydrogels by incorporation of neat laponite RD clay. The adsorption of CV onto HPMC/laponite RD and kappa-carrageenan/laponite RD nanocomposite hydrogels showed that the experimental isotherm data followed well Langmuir model and maximum adsorption capacities were obtained 80.2 and 77 mg g^{-1} for kappa-carrageenan/laponite RD [23] and HPMC/laponite RD [32], respectively. In this study, the experimental adsorption capacities of mCMC-*g*-PAAmLap1, mCMC-*g*-PAAmLap2, mCMC-*g*-PAAmLap3, and mCMC-*g*-PAAmLap4 for CV were obtained 120, 132, 153, and 169 mg g^{-1}, respectively. Thus, the following adsorption isotherm data from Freundlich and subsequent multilayer adsorption of CV on samples (against monolayer adsorption in Langmuir model) may be a reason for enhanced dye adsorption capacity of present samples [3].

Thermodynamic parameters

Thermodynamic parameters should be considered as important factors in the design of adsorption process. It is necessary to specify the change of thermodynamic parameters to estimate the feasibility and mechanism of adsorption process [35]. Thermodynamic parameters including standard Gibbs free energy (ΔG, J mol^{-1}), enthalpy change (ΔH, J mol^{-1}), and entropy change (ΔS, J K^{-1} mol^{-1}) are calculated according to the following equations [38]:

$$\ln K_C = -\frac{\Delta H}{RT} + \frac{\Delta S}{R}, \tag{7}$$

$$\Delta G = \Delta H - T\Delta S \tag{8}$$

$$K_c = \frac{q_e}{C_e}, \tag{9}$$

where K_c is the equilibrium constant; q_e is the dye adsorbed onto nanocomposite (mg L^{-1}) and C_e is the equilibrium concentration of dye in solution (mg L^{-1}); R is the universal gas constant (8.314 J mol^{-1} K^{-1}); and T is the absolute temperature (K). ΔH and ΔS were calculated from slope and intercept of linear plot of ln K_c versus *1/T*, respectively (Eq. 7). ΔH and ΔS values for mCMC-*g*-PAAmLap2 were obtained 23.5 kJ mol^{-1} and 113 J K^{-1} mol^{-1}, respectively (Table 4). While the positive value of ΔH indicates the endothermic nature of adsorption process, the positive value of enthalpy shows that during the adsorption of dye onto the nanocomposite, an increased randomness at the solid–solution interface is occurred. The Gibbs free energy for the adsorption of CV on mCMC-*g*-PAAmLap2 was obtained −9.7, −10.6, and −11.98 kJ mol^{-1} at 285, 295, and 305 K, respectively. The negative values of ΔG showed a spontaneous adsorption process. By increasing

Table 4 Thermodynamic parameters for adsorption of CV on mCMC-*g*-PAAmLap2 nanocomposite

T (K)	ΔS (J K^{-1} mol^{-1})	ΔH (kJ mol^{-1})	ΔG (kJ mol^{-1})	R^2
285	+113	+23.5	−9.7	0.95
295			−10.6	
305			−11.98	

of the temperature, the values of ΔG showed more negative values, showing the more favorability of adsorption of CV on adsorbent.

The mechanism of adsorption of dye on nanocomposites could be estimated from the values of ΔG and ΔH [39, 40]. The values of ΔG ranging from −20 to 0 kJ mol^{-1} indicate that the physisorption is dominated; but chemisorption is occurred for a range of −80 to −400 kJ mol^{-1}. By considering the data of Table 4, it is concluded that in this study, the mechanism of adsorption process is physisorption. In addition, the values of ΔH lower than 20 kJ mol^{-1} depicts that the physisorption interactions such as Van der Waals are dominated. The values of ΔH ranging from 20 to 80 kJ mol^{-1} indicate that the physisorption interaction such as electrostatic leads to adsorption of adsorbate on adsorbent. The chemisorption interaction occurs when the values of ΔH are between 80 and 450 kJ mol^{-1}. The enthalpy value for the adsorption of CV on magnetic nanocomposite was obtained 23.5 kJ mol^{-1}. According to the ΔH value for the adsorption process, the positive CV dye molecules adsorb electrostatically on the anionic centers of magnetic nanocomposite.

Desorption–adsorption cycles

By increasing the cost-effectiveness of adsorbents, desorption of adsorbed dye should be considered as an important factor to reuse adsorbents. Therefore, using different solutions, the regeneration of magnetic hydrogel mCMC-*g*-PAAmLap4 was evaluated. Ethanol (96 % v/v), 0.2 M of acetic acid solution, 0.5 M of KCl solution, 50/50 v/v of ethanol/water mixture, and 0.5 M of KCl in 50/50 v/v of ethanol/water mixture were used for desorbing of dye from hydrogels. Desorption efficiencies by various solutions are illustrated in Fig. 6a. First of all, the desorbing adsorbed dye was examined by 0.2 M acetic acid solution and desorption efficiency was low ($\sim$20 %). The desorbing of dye in the presence of acetic acid can be attributed to the protonation of carboxylate groups on carboxymethyl chitosan. Then, desorption was examined with 0.5 M KCl solution and the desorbing of dye was negligible. The desorbing percentage of dye using 96 % v/v of ethanol was obtained 43 %. By replacing desorption solution by ethanol/water mixture (50/50 v/v), desorption efficiency was achieved 27 %. Desorption efficiency of dye using above solutions was not sufficient for practical applications. So, we tried to investigate the desorbing of dye by combination of KCl and ethanol/water mixture. By immersing the nanocomposite containing dye into 0.5 M of KCl in ethanol/water, desorption efficiency was efficiently increased and obtained more than 97 %.

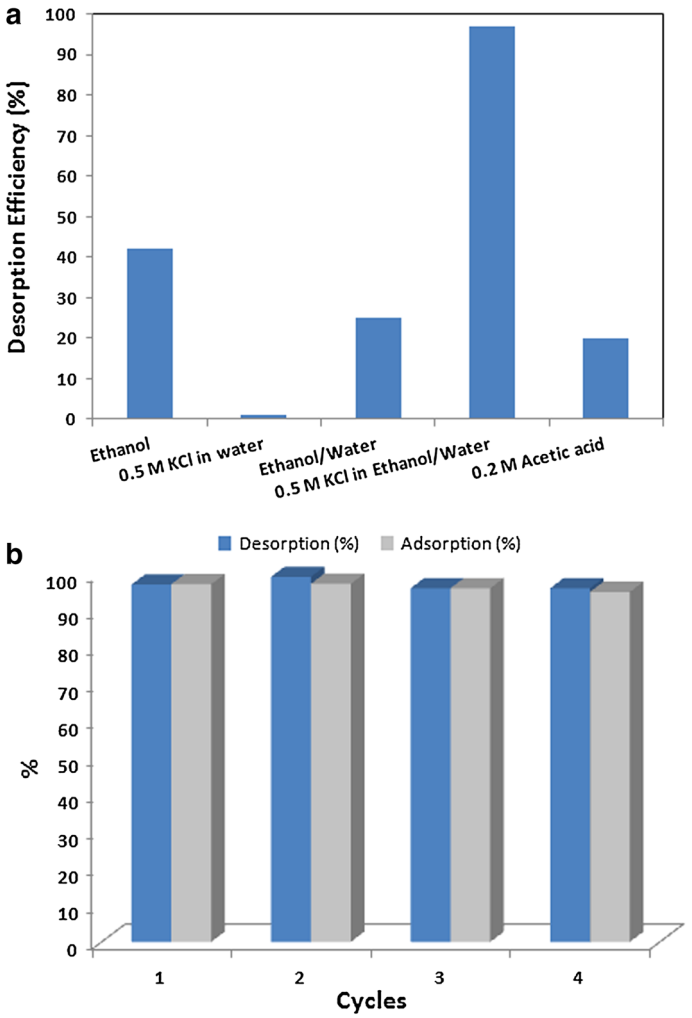

Fig. 6 **a** Effect of type of desorption solution on the desorption of dye from mCMC-*g*-PAAmLap4 nanocomposite hydrogel, **b** reuse of mCMC-*g*-PAAmLap4 magnetic nanocomposite hydrogel using 0.5 M KCl in ethanol/water solution

According to this observation, we endeavored to study the desorption–adsorption process for 4 cycles using the 0.5 M KCl in ethanol/water as regeneration agent and the results are shown in Fig. 6b. During four cycles, the nanocomposite indicated almost the same dye adsorption capacity and the change in desorption efficiency and adsorption capacity was negligible. In fact, the results indicated that the nanocomposites can be used for multiple cycles without decrease in adsorption capacity for CV dye.

Conclusion

In this work, adsorption of cationic dye CV on magnetic nanocomposite hydrogels was investigated. The magnetic hydrogels were synthesized by grafting poly(acrylamide) on carboxymethyl chitosan and by incorporating magnetic laponite RD. Magnetic clay was obtained through in situ co-precipitation of iron ions in the presence of laponite RD. It was observed that the water absorbency of magnetic nanocomposites was affected by the content of magnetic laponite RD. In distilled water, the swelling capacity was decreased by increasing the magnetic clay. Salt sensitivity of nanocomposites was decreased as the magnetic laponite RD increased. Dye adsorption results revealed that the removal of dye was strongly increased by introducing magnetic laponite RD. Also, increase in the content of magnetic clay caused an enhancement in dye adsorption capacity of nanocomposites under acidic media. The batch adsorption experimental data were analyzed according to Freundlich and Langmuir models. By incorporation of magnetic laponite RD, the following experimental adsorption isotherm data deviated from Langmuir to Freundlich. According to thermodynamic parameters, the adsorption of CV dye on adsorbents occurred spontaneously. The results demonstrated that the nanocomposites can be used for multiple cycles without decreasing the adsorption capacity for CV.

References

1. Crini G (2006) Non-conventional low-cost adsorbents for dye removal: a review. Bioresour Technol 97:1061–1085
2. Mondal S (2008) Methods of dye removal from dye house effluent: an overview. Environ Eng Sci 25:383–396
3. Zheng Y, Wang A (2010) Preparation and ammonium adsorption properties of biotite-based hydrogel composites. Ind Eng Chem Res 49:6034–6041
4. Belaid KD, Kacha S, Kameche M, Derriche Z (2013) Adsorption kinetics of some textile dyes onto granular activated carbon. J Environ Chem Eng 1:496–503
5. Elsherbiny AS (2013) Adsorption kinetics and mechanism of acid dye onto montmorillonite from aqueous solutions: stopped-flow measurements. Appl Clay Sci 83–84:56–62
6. Mahdavinia GR, Baghban A, Zorofi S, Massoudi A (2014) kappa-Carrageenan biopolymer based nanocomposite hydrogel and adsorption of methylene blue cationic dye from water. J Mater Environ Sci 5:330–337
7. Mahdavinia GR, Asgari A (2013) Synthesis of kappa-carrageenan-g poly(acrylamide)/sepiolite nanocomposite hydrogels and adsorption of cationic dye. Polym Bull 70:2451–2470
8. Hamid M, Azadi A, Rafiei P (2008) Hydrogel nanoparticles in drug delivery. Adv Drug Deliv Rev 60:1638–1649
9. Mahmoodi NM, Hayati B, Arami M, Bahrami H (2011) Preparation, characterization and dye adsorption properties of biocompatible composite (alginate/titania nanoparticle). Desalination 275:93–101
10. Saber-Samandari S, Saber-Samandari S, Nezafati N, Yahya K (2014) Efficient removal of lead (II) ions and methylene blue from aqueous solution using chitosan/Fe-hydroxyapatite nanocomposite beads. React Funct Polym 146:481–490
11. Bhatnagar A, Sillanpaa M (2009) Applications of chitin- and chitosan-derivatives for the detoxification of water and wastewater-A short review. Adv Colloid Interface Sci 152:26–38

12. Wang L, Wang A (2008) Adsorption properties of congo red from aqueous solution onto N, O-carboxymethyl-chitosan. Bioresour Technol 99:1403–1408
13. Wang L, Lim Q, Wang A (2010) Adsorption of cationic dye on *N*,*O*-carboxymethyl-chitosan from aqueous solutions: equilibrium, kinetics, and adsorption mechanism. Polym Bull 65:961–975
14. Wang F, Zhao J, Zhou H, Li W, Sui N, Lin H (2013) *O*-Carboxymethyl chitosan entrapped by silica: preparation and adsorption behaviour toward neodymium (III) ions. J Chem Technol Biotechnol 88:317–325
15. Wang L, Wang A (2008) Adsorption behaviors of Congo red on the N, O-carboxymethyl-chitosan/montmorillonite nanocomposite. Chem Eng J 143:43–50
16. Sabaa MW, Mohamed RR, Eltaweel SH, Seoudi RS (2012) Crosslinked poly(vinyl alcohol)/carboxymethyl chitosan hydrogels for removal of metal ions and dyestuff from aqueous solutions. J Appl Polym Sci 123:3459–3469
17. Pourjavadi A, Hosseini SH, Seidi F, Soleyman R (2013) Magnetic removal of crystal violet from aqueous solutions using polysaccharide-based magnetic nanocomposite hydrogels. Polym Int 62:1038–1044
18. Mahdavinia GR, Iravani S, Zoroufi S, Hosseinzadeh H (2014) Magnetic and K^+-cross-linked kappa-carrageenan nanocomposite beads and adsorption of crystal violet. Iran Polym J 23:335–344
19. Bruce IJ, Sen T (2005) Surface modification of magnetic nanoparticles with alkoxysilanes and their application in magnetic bioseparations. Langmuir 19:7029–7035
20. Wu D, Zheng P, Chang PR, Ma X (2011) Preparation and characterization of magnetic rectorite/iron oxide nanocomposites and its application for the removal of the dyes. Chem Eng J 174:489–494
21. Jiang L, Liu P (2014) Design of magnetic attapulgite/fly ash/poly(acrylic acid) ternary nanocomposite hydrogels and performance evaluation as selective adsorbent for Pb^{2+} ion. ACS Sustain Chem Eng 2:1785–1794
22. Mahdavinia GR, Massoudi A, Baghban A, Shokri E (2014) Study of adsorption of cationic dye on magnetic kappa-carrageenan/PVA nanocomposite hydrogels. J Environ Chem Eng 2:1578–1587
23. Mahdavinia GR, Massoudi A, Baghban A, Massoumi B (2012) Novel carrageenan-based hydrogel nanocomposites containing laponite RD and their application to remove cationic dye. Iran Polym J 21:609–619
24. Sun P, Zhang H, Liu C, Fang J, Wang M, Chen J, Zhang J, Mao C, Xu S (2010) Preparation and characterization of Fe_3O_4/CdTe magnetic/fluorescent nanocomposites and their applications in immuno-labeling and fluorescent imaging of cancer cells. Langmuir 26:1278–1284
25. Tzitzios V, Basina G, Bakandritsos A, Hadjipanayis CG, Mao H, Niarchos D, Hadjipanayis GC, Tucek J, Zboril R (2010) Immobilization of magnetic iron oxide nanoparticles on laponite discs—an easy way to biocompatible ferrofluids and ferrogels. J Mater Chem 20:5418–5428
26. Goiti E, Salinas MM, Arias G, Puglia D, Kenny JM, Mijangos C (2007) Effect of magnetic nanoparticles on the thermal properties of some hydrogels. Polym Degrad Stabil 92:2198–2205
27. Mahdavinia GR, Marandi GB, Pourjavadi A, Kiani G (2010) Semi-IPN carrageenan-based nanocomposite hydrogels: synthesis and swelling behavior. J Appl Polym Sci 118:2989–2997
28. Philippova O, Barabanova A, Molchanov V, Khokhlov A (2011) Magnetic polymer beads: recent trends and developments in synthetic design and applications. Eur Polym J 47:542–559
29. Mahdavinia GR, Pourjavadi A, Hosseinzadeh H, Zohuriaan MJ (2004) Modified chitosan 4. Superabsorbent hydrogels from poly(acrylic acid-co-acrylamide) grafted chitosan with salt- and pH-responsiveness properties. Eur Polym J 40:1399–1407
30. Darvishi Z, Kabiri K, Zohuriaan-Mehr MJ, Morsali A (2011) Nanocomposite super-swelling hydrogels with nanorod bentonite. J Appl Polym Sci 120:3453–3459
31. Mahdavinia GR, Zohuriaan-Mehr MJ, Pourjavadi A (2004) Modified chitosan III, superabsorbency, salt- and pH-sensitivity of smart ampholytic hydrogels from chitosan-*g*-PAN. Polym Adv Technol 15:173–180
32. Mahdavinia GR, Bazmizeynabad F (2014) Synthesis of anti-salt hydroxypropyl methylcellulose-*g*-polyacrylamide/laponite RD nanocomposite hydrogel and its application to remove cationic dye. Polym-Palst Technol 53:411–422
33. HuY Guo T, Ye X, Li Q, Guo M, Liu H, Wu Z (2013) Dye adsorption by resins: effect of ionic strength on hydrophobic and electrostatic interactions. Chem Eng J 228:392–397
34. Gusmao KAG, Gurgel LVA, Melo TMS, Gil LF (2013) Adsorption studies of methylene blue and gentian violet on sugarcane bagasse modified with EDTA dianhydride (EDTAD) in aqueous solutions: kinetic and equilibrium aspects. J Environ Manage 118:135–143

35. Tang H, Zhou W, Zhang L (2012) Adsorption isotherms and kinetics studies of malachite green on chitin hydrogels. J Hazard Mater 290–210:218–225
36. Foo KY, Hameed BH (2010) Insights into the modeling of adsorption isotherm systems. Chem Eng J 156:2–10
37. Hameed BH, Ahmad AA, Aziz N (2007) Isotherms, kinetics and thermodynamics of acid dye adsorption on activated palm ash. Chem Eng J 133:195–203
38. Auta M, Hameed BH (2011) Preparation of waste tea activated carbon using potassium acetate as an activating agent for adsorption acid blue 25 dye. Chem Eng J 171:502–509
39. Ozcan A, Oncu EM, Ozcan S (2006) Adsorption of acid blue 193 from aqueous solutions onto DEDMA-sepiolite. J Hazard Mater B129:244–252
40. Machado FM, Bergmann CP, Fernandes THM, Lima EC, Royer B, Calvete T, Fagan SB (2011) Adsorption of Reactive Red M-2BE dye from water solutions by multi-walled carbon nanotubes and activated carbon. J Hazard Mater 192:1122–1131